RSC Advances

ROYAL SOCIETY OF CHEMISTRY

www.rsc.org/advances

RSC Advances

RSCPublishing

ARTICLE

Anomalous Variation of Electrical Transport Property and Amorphization in Dense Alq_3

Feng Ke,[a,b] Qinglin Wang,[b] Junkai Zhang,[b] Ying Guo,[a] Dayong Tan,[b,c] Yan Li,[a] Cailong Liu,*[a] Yonghao Han,[a] Yanzhang Ma,[d] Xiao-Jia Chen,[b] Bin Chen[b] and Chunxiao Gao*[a]

Cite this: DOI: 10.1039/xoxxoooooox

Received ooth January 2015,
Accepted ooth January 2015

DOI: 10.1039/xoxxoooooox

www.rsc.org/

We report intriguing electrical transport and structural properties on compressed Alq_3, an extensively used electron transport material in OLED. The bulk resistance (R_b) of Alq_3 increases with uploading pressure, but drops markedly above 8.6 GPa. By contrast the grain boundary resistance (R_{gb}) varies smoothly below 16.4 GPa. With further compression, both of R_b and R_{gb} increase with the amorphization of Alq_3. Pressure-induced amorphization is found reversible at low density amorphous state while irreversible at higher density state. Interestingly, XRD measurements indicate no structural transition at ~8.0 GPa. The variation of R_b is found synchronous with the blue-shift of Al-oxine deformation mode, which rationalizes the anomalous changes of R_b. The Al-oxine interaction is believed also significant on electrical transport properties of dense Alq_3, which provides insight into the correlation between structural change and electrical transport properties.

Introduction

Since the first discovery of tris (8-hydroxyquinoline) aluminum (Alq_3)-based multilayer thin-film electroluminescent devices by Tang and co-authors in 1987,[1] much progress has been made on its application of the organic light-emitting devices (OLEDs) as electron-transporting materials.[2-6] Besides the optimization of Alq_3-based devices with higher efficiency and long-term stability, much theoretical and experimental effort focus on the polymorphs and photo-physics properties of Alq_3.[7-15] At room conditions, Alq_3 crystallizes into an octahedral coordinated chelate complex with Al^{3+} at the center and three 8-hydroxyquinoline ions around, which generally adopts two types of geometrical isomeric forms, namely, meridional isomeric form (mer-Alq_3) with C_1 symmetry and facial isomeric from (fac-Alq_3) with C_3 symmetry, depending on the orientation of the ligands.[15-22] The structural difference between these two isomers is small, but quite different physical properties such as color and fluorescence have been observed. The green emission for light-yellow mer-Alq_3 and blue emission for whitish fac-Alq_3 have been attracting intensive interest of the scientists in functional material area.

Recently, the spectral position of fluorescence of Alq_3 was found to be correlated with both the molecular packing density and the length of interligand contacts between its neighboring molecular as a consequence of different dispersive and dipolar interactions as well as different π-π orbital overlapping, that is, the denser the crystal is, the more red-shifted the fluorescence is.[15] This π-π stacking interaction is also considered as a key factor for the electrical transport properties of Alq_3, one of the most important physical properties in optimizing or designing new applications of organic functional material.[9,12-14] For instance, in Alq_3, large intermolecular electronic interaction, which depends on both intra- and intermolecular structures, is critical to the charge transfer rate and charge mobility.[13] An important issue concerns how to alter the optical and electrical transport properties of Alq_3 by tuning the intra- and intermolecular structure with external stimuli (*e.g.* pressure /temperature). As well known, compression is a powerful tool to drive transformation toward the structures with higher density without inducing impurity or changing the chemical nature of materials,[23] providing an approach to further explore the correlation between the structural and other physical properties of Alq_3. Previous studies verified that the photoluminescence spectra of Alq_3 were indeed red-shifted largely more than 0.3 eV.[24-26] Changes of electronic structure can affect electrical transport property of material fundamentally. Nevertheless, it remains unclear how compression tunes the transport behavior of Alq_3, limiting to design new Alq_3-based applications. Another factor that critically affects the performance of OLEDs lighting or display application is grain boundary or interface of crystalline materials. Carrier scattering effect is usually strengthened at grain boundaries, and thus changes the electrical transport properties of materials. The effect of grain boundary on the electrical transport properties of Alq_3 under compression is underinvestigated and thus poorly understood.

An effective approach to solve above mentioned issues is the alternating current electrical response analysis, *i.e.*, frequency-dependent impedance spectroscopy, by which the contribution of bulk and grain boundary effect on total electrical transport properties can be distinguished. Furthermore, in situ high-pressure synchrotron X-ray diffraction (XRD) and Raman spectra were conducted to monitor the structural modification, which is still not well-defined but of great importance for understanding the changes of physical properties of Alq_3 under compression. Besides, high-resolution

transmission electron microscopy (TEM) is applied to observe the pressure-induced change on grain boundary of Alq_3. By combining these measurements, we have studied the electrical transport and structural properties of Alq_3 under compression.

Experimental Section

Alternating current impedance spectroscopy measurements consist of a time (t)-dependent alternating voltage signal $U(\omega,t) = U_0 \cos(\omega t)$ applied to a sample, and the current response signal I are determined, $I(\omega,t) = I_0 \cos(\omega t-\gamma)$, where ω, U_0, I_0 and γ are angular frequency, voltage amplitude, current amplitude and phase shift, respectively. Then one can obtain complex impedance $Z^* = U/I = Z' + iZ''$, in which the impedance fraction in phase with $U(\omega,t)$ is defined as the real (Z') and the $\pm\pi/2$ out of phase part is defined as the positive/negative imaginary part (Z''), respectively. In our experiments, a.c. voltage signal with amplitude of 2 V and frequency ranged from 0.01 to 10^7 Hz was applied to the samples. Solartron 1260 impedance analyzer interfaced with Solartron 1296 dielectric interface were used to detect the impedance spectra. Impedance spectra were measured with two-electrode configuration microcircuit, Mo film electrode used as one of the probing electrodes and the sidewall of sample chamber as the other. T301 steel was used as the gasket. Fabrication of Mo film microcircuit on diamond surface, insulating method between gasket and Mo film electrode, and other experimental details were reported previously.[27,28]

In situ high-pressure XRD measurements on Alq_3 were conducted at beamline 4W2 of Beijing Synchrotron Radiation Facility (BSRF) and 15U1 of Shanghai Synchrotron Radiation Facility (SSRF) using angle-dispersive XRD source (λ = 0.6199 Å). Powdered Alq_3 samples (bought from Sigma-Aldrich Co.) and a small piece of ruby as the pressure calibrant[29] were loaded into a diamond-anvil cell. Silicone oil was used as pressure transmitting medium. Distance between sample and detector, and parameters of detector were calibrated using a CeO_2 standard. Bragg diffraction images were integrated using Fit2d software, yielding one-dimensional intensity versus diffraction angle 2θ patterns. High-pressure Raman spectra were collected with Renishaw InVia spectrometer using a 633 nm He-Ne laser and a 50 times Leica optical microscope.

Results and discussion

Shown in Fig. 1 is the impedance spectra data of Alq_3 powders with pressure up to 19.4 GPa as the imaginary part of complex impedance (Z'') plotted vs that of the real part (Z'). It is found that, unlike previously reported impedance spectroscopy observations where two semicircles describing the bulk and grain boundary effect can be distinguished clearly in the complex plane,[30] only one strongly suppressed arc is observed in our experimental results. But the curvature of the left high-frequency arc is larger than that of the right low-frequency arc. This observation can be attributed to the strong overlapping of the bulk and grain boundary semicircles due to the similar time constants between these two relaxations processes.[31] The left high-frequency and right low-frequency components correspond to the bulk and grain boundary effect, respectively.[32,33] The straight line at the right corner of the complex impedance should be a consequence of the contact effect among the sample and Mo film microcircuits.[34]

To quantify the pressure effect on the electrical transport properties of Alq_3, the impedance spectra were fitted with a commonly equivalent circuit model, in which two parallel resistors (R) and constant-phase elements (CPE) (Fig. 1b) are introduced to describe the bulk and grain boundary relaxation processes, respectively, on Zview2 impedance analysis software. The non-ideality of the complex impedance is accounted for by the use of CPE elements, which may affect the reliability of capacitance or inductance value, while the resistance remains unaffected. The obtained bulk (R_b) and grain boundary resistances (R_{gb}) are plotted in Fig. 1d. R_b of Alq_3 increases markedly at low pressures (< 3.1 GPa), followed by a shoulder from 3.1 to 5.7 GPa, and continues the increasing tendency up to 7.9 GPa. However, with continuous compression the pressure dependence turns around and R_b drops rapidly below 15.9 GPa. Similar shoulder in the pressure range of 3.1~6.1 GPa has also been observed in the photoluminescence spectra of Alq_3.[25,26] By contrast, R_{gb} varies smoothly below 16.4 GPa. Above 16.4 GPa, both R_b and R_{gb} increase dramatically with pressure.

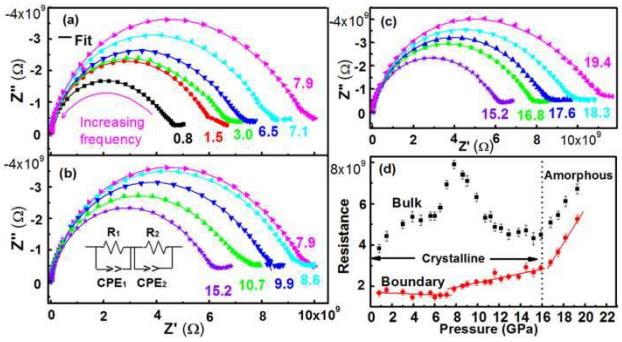

Fig.1 (a)-(c) Complex impedance plots of Z'' vs Z' of Alq_3 under compression. Lines are the fitted results with the equivalent circuit models describing the bulk (R_1-CPE_1) and grain boundary (R_2-CPE_2) effects shown in inset of Figure 1b. The fitting error is less than 5%. (d) Pressure dependence of the obtained bulk and grain boundary resistances of Alq_3.

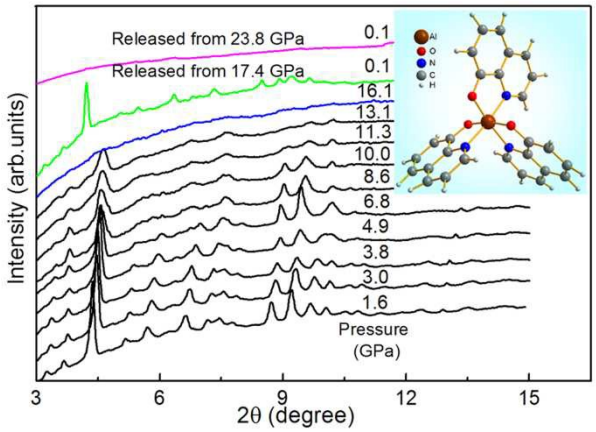

Fig. 2 Representative XRD patterns of Alq_3 at various pressures (λ = 0.6199 Å). The inset shows the structural model of Alq_3.

We were motivated to find out the mechanism behind the anomalous variation of the electrical transport properties of Alq_3 under compression. Discontinuous variation of electrical transport property of materials usually coincide with the instability of crystal structure.[35,36] High-pressure XRD measurements were conducted on Alq_3 up to 17.4 GPa for in situ observation of the structural modification. The selected patterns are shown in Fig. 2. At room conditions, triclinic crystal structure with P-1 symmetry (β-Alq_3) seems more suitable for the structure of Alq_3. The inset of Fig. 2 shows the structure model of Alq_3. It is surprising that, below 16.1 GPa, there is no obvious variation on the patterns of Alq_3 except the relative peak broadening and the collective movements of all reflection peaks toward lower d-spacing. Above 16.1 GPa, all the diffraction peaks lose their intensity, indicating that Alq_3 becomes

amorphous. After quenching to ambient pressure, all of the reflection peaks re-emerge (Fig. 2), indicating that the amorphization process is reversible. However, it is found that when the sample is pressurized up to 23.8 GPa and then quenched to ambient pressure the pattern remains disappeared, showing the irreversible character.

To further explore the mechanism behind and probe the subtle changes of the structures, we conducted high-pressure Raman spectra measurements on Alq_3. As shown in Figs. 3 and 4, in the low pressure range, 0.3~6.9 GPa, no obvious change but the blue-shift, varied relative intensity, and broadening of the vibration Raman modes can be observed. However, above 8.6 GPa, the low-frequency vibration modes in the range of 50 to 200 cm^{-1} lose their intensity. The disappearance tendency expands to higher-frequency vibration modes in the further compression process. All the Raman vibration modes disappear at ~17.7 GPa. In the decompression, the lost Raman vibration modes of Alq_3 reappear when the sample was decompressed from 17.7 GPa, but remain disappeared when decompressed from 23.4 GPa, which agrees well with the XRD observation that Alq_3 becomes amorphous above 16.1 GPa, and the amorphous process is reversible in the compression below 17.4 GPa but irreversible if compressed to higher pressure, *e. g.* 23.8 GPa. This observation can be attributed to the crystalline topology effect.[37,38] At relative low pressure, the crystalline topology of Alq_3 (including the atomic coordination and bonding) is preserved, which retains a "memory" of its original crystal structure and can revert to it when releasing pressure to ambient conditions. Upon further compression, the relative higher density amorphous state can be achieved which involves some bonding breaking, and the broken bonding cannot recover to its original state in decompression. Consequently the pressure-induced amorphization shows irreversible character.

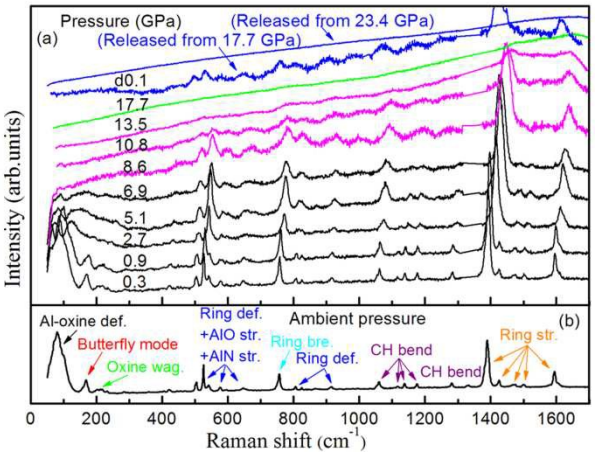

Fig. 3 High-pressure Raman spectra of Alq_3 with the Raman peaks of diamond at ~1331 cm^{-1} subtracted. Here the def., wag., str., and bre. represent the deformation, wagging, stretching, and breathing vibration modes, respectively.

Raman studies revealed the subtle structural changes of Alq_3 under pressure. At room conditions, the Raman vibration modes of Alq_3 have been well assigned [39,40] (Fig. 3b). As clearly shown in Fig. 4, above 8.0 GPa, the Raman active modes lose their intensity gradually from low- to high-frequency range, indicating that the Al-oxine bonding is firstly tuned, and then the oxine ligands lose their long-distance ordering, followed by the modification of the ring and C-H bonds with increasing pressure. We infer that the relative Raman intensity changes of the Al-oxine vibration modes (Fig. 4) are caused by the pressure-induced modification of the Al-oxine bonding and the non-planar conformation of the Alq_3 molecules. Application of pressure promotes the molecular modification from a non-planar to a planar state, which was observed on other non-planar metal-organic frameworks in previous studies.[41,42]

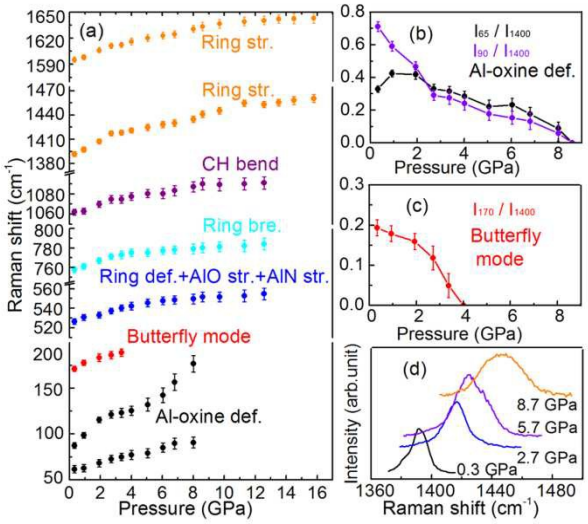

Fig. 4 (a) Pressure dependence of Raman peaks positions of Alq_3. (b) and (c) The ratio of the intensity of the ~65 cm^{-1}, ~90 cm^{-1}, and ~170 cm^{-1} Raman vibration modes to the ~1400 cm^{-1} mode in Alq_3 as a function of pressure. (d) The variation of the Raman peak width (~1400 cm^{-1}) under pressure.

To further study the effect of compression on the grain boundary, we performed high-resolution transmission electron microscopy (TEM) on Alq_3, which can directly inspect the detailed atomic information, and hence is reliable to identify the grain boundaries. Figure 5 shows the TEM observation of samples that decompressed from 7, 11 and 17 GPa, respectively. It can be found that the average grain size of Alq_3 changes smoothly from ambient pressure to 7 GPa, while decreases significantly at 11 GPa, and becomes smaller at 17 GPa, indicating the increase of grain boundary density with applying compression.

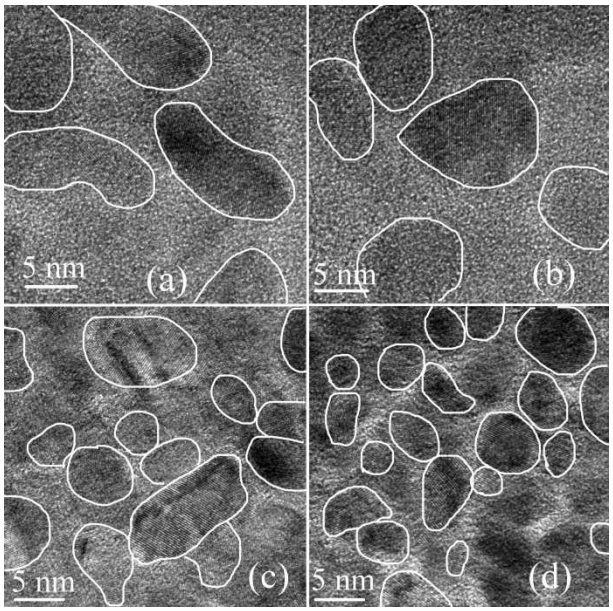

Fig. 5. High-resolution transmission electron microscope of Alq_3 quenched from different pressures: (a) ambient pressure, (b) 7 GPa, (c) 11 GPa and (d) 17 GPa, respectively.

The information about the structural evolution under compression is helpful for understanding the complicated electrical transport properties of Alq_3. In the low pressure region (below 8.0 GPa), the crystal structure of Alq_3 remains relatively stable. Hence the grain boundary density should be dynamically balanced, and the boundary carrier scattering effect keeps almost unchanged. Consequently, R_{gb} varies smoothly with pressure. Above 8.0 GPa, the Al-oxine deformation modes of Alq_3 lose their intensity, signaling the essential changes of Al-oxine bonding. The bonding changes connect with the deformation of the Alq_3 molecules, and subsequently affect the grain boundary density and the grain boundary disordering, which strengthen the boundary charge carrier scattering effect, and accordingly R_{gb} of Alq_3 increases gradually with pressure. Above 16.4 GPa, Alq_3 becomes amorphous, resulting in the sharp increase of the grain boundary density and the structural disordering. As a consequence, the charge carrier scattering effect of grain boundary is strengthened, and which further hinders the boundary conduction of Alq_3.

In case of bulk electrical transport, it is shown in previously reported studies that the π-π stacking interaction play important roles on the electrical transport properties of Alq_3.[9,13-14] Under compression, the π-π stacking interaction is modified, which is critical to increase the charge transfer rate and charge mobility, and hence facilitate the electrical transport of Alq_3.[13] Therefore the electrical conductivity of Alq_3 should be improved, while it is not consistent with the measured R_b of Alq_3 in the compression at 1.6~7.9 GPa. We infer that besides the above mentioned factor, some other factors also affect the electrical transport properties of Alq_3. The similar change tendency between the Al-oxine deformation mode (at ~90 cm^{-1}, shown in Fig. 4) and R_b below 8.0 GPa is the hint of their correlation. Another evidence to support their correlation can be observed from Ref 10 that the bonding lengths and angles between central cation and oxine ligand can heavily affect the electronic structure.[10] This observation can be understood as following: at ambient pressure, the sample has the low symmetry of crystal structure that the three Al-oxine ligands (including the Al-O and Al-N bonds) each has different bond lengths and angles, and the charges are not uniformly localized on three ligands.[8] The bonding conformation makes the Al-oxine interaction sensitive to pressure. Under compression, the Al-oxine bonding, especially the Al-N and Al-O bonding lengths and angles are modified obviously, which may enhance the localization of the charge carriers, and so hinder the conduction of Alq_3. Moreover, pressure-induced defects and structural disordering, reflected in the broadening in the Raman spectra and XRD peaks of Alq_3 under compression, usually trap the charge carriers and act as recombination centers and can also affect the electrical transport properties of Alq_3. Thus, R_b of Alq_3 increases with uploading pressure. Above 8.0 GPa, the essential changes of Al-oxine interaction fundamentally modify the electronic structure of Alq_3, driving the redistribution of electron density between adjacent oxine ligands and the localized-delocalized charger transfer, which combine with the improved conduction due to the enhanced π-π stacking interaction and non-planar to more-planar conformation modification under compression, offsets the hindering effect of structural disorder or defects and makes Alq_3 more conductive. The dramatic increase of R_b above 16.4 GPa is induced by the amorphization process, which brings about a higher degree of structural disorder and significantly reduced the free travelling distances of the charge carriers. The experiment results suggest that the Al-oxine interaction also plays an important role on the electrical transport properties of Alq_3.

Conclusions

By combing the XRD, Raman spectra, TEM and impedance spectra measurements, we have studied the electrical transport and structural properties of compressed Alq_3, an extensively used electron transport material in OLEDs. R_b of Alq_3 increases with uploading pressure, while drops markedly above 8.6 GPa. By contrast, R_{gb} changes smoothly below 16.4 GPa. With further compression, both R_b and R_{gb} increase dramatically along with the amorphization of Alq_3. Pressure-induced amorphization is reversible at low density amorphous state but irreversible at relative higher density state. Interestingly, XRD measurements indicate no structural transition at ~ 8.0 GPa, the pressure that R_b reaches maximum. The tendency reversal is found synchronous with the Raman shift of the Al-oxine deformation vibration modes, which rationalizes the anomalous changes of the electrical transport behavior. Besides the contribution of π-π stacking interaction, Al-oxine interaction is believed also important on the transport properties on dense Alq_3, which provides essential insight into the correlation between structural modification and electrical properties, and establishes general guidelines in designing or optimizing new Alq_3-based applications.

Acknowledgements

The authors thank M. Zhou (College of physics, Jilin University, China) for discussion. This work was supported by the National Basic Research Program of China (Grant No. 2011CB808204), the National Natural Science Foundation of China (Grant Nos., 11374121 and 11404133), the China Postdoctoral Science Foundation (Grant No. 2013M540243), and the Program of Science and Technology Development Plan of Jilin Province (Grant No. 20140520105JH).

Notes and references

[a] State Key Lab for Superhard Materials, Institute of Atomic and Molecular Physics, Jilin University, Changchun 130012, China. E-mail: cailong_liu@jlu.edu.cn; gaocx@jlu.edu.cn

[b] Center for High Pressure Science and Technology Advanced Research, Shanghai 201203, China.

[c] Guangzhou Institute of Geochemistry, Chinese Academy of Sciences, Guangzhou 510640, China.

[d] Department of Mechanical Engineering, Texas Tech University, Lubbock, TX 79409, USA.

1 C. W. Tang, S. A. VanSlyke, *Appl. Phys. Lett.*, 1987, **51**, 913.
2 J. M. Shi, C. W. Tang, *Appl. Phys. Lett.*, 1997, **70**, 1665.
3 H. Aziz, Z. D. Popovic, *Chem. Mater*., 2004, **16**, 4522.
4 S. Berleb, W. Brutting, *Phys. Rev. Lett.*, 2002, **89**, 286601.
5 H. Aziz, Z. D. Popovic, N. X. Hu, A. M. Hor, G. Xu, *Science*, 1999, **283**, 1900.
6 M. S. Xu, J. B. Xu, *Thin Solid Films*, 2005, **491**, 317.
7 M. Muccini, M. A. Loi, K. Kenevey, R. Zamboni, N. Masciocchi, A. Sironi, *Adv. Mater.*, 2004, **16**, 861.
8 A. Curioni, M. Boero, W. Andreoni, *Chem. Phys. Lett.*, 1998, **294**, 263.
9 B. C. Lin, C. P. Cheng, Z. Q. You, C. P. Hsu, *J. Am. Chem. Soc*., 2005, **127**, 66.
10 F. F. Muhammad, A. I. A. Hapip, K. *J.* Sulaiman, *Organomet. Chem.*, 2010, **695**, 2526.
11 M. Rajeswaran, T. N. Blanton, *J. Chem. Crystallogr.*, 2005, **35**, 71.
12 J. S. Jiang, J. E. Pearson, S. D. Bader, *Phys. Rev. B*, 2008, **77**, 035303.
13 B. C. Lin, C. P. Cheng, Z. Q. You, C. P. Hsu, *Phys. Chem. Chem. Phys.*, 2011, **13**, 20704.
14 A. Fuchs, T. Steinbrecher, M. S. Mommer, Y. Nagata, M. Elstner; C. Lennartz, *Phys. Chem. Chem. Phys.* 2012, **14**, 4259.
15 M. Brinkmann, G. Gadret, M. Muccini, C. Taliani, N. Masciocchi, Sironi, A. *J. Am. Chem. Soc.* 2000, **122**, 5147.

16 M. Colle, R. E. Dinnebier, Brutting, W. *Chem. Comm.* 2002, 2908.
17 H. Bi, D. Chen, D. Li, Y. Yuan, D. D. Xia, Z. L. Zhang, H. Y. Zhang, Y. Wang, *Chem. Comm.*, 2011, **47**, 4135.
18 M. Goswami, P. K. Nayak, N. Periasamy, P. K. Madhu, *Chem. Cent. J.*, 2009, **3**, 15.
19 M. Rajeswaran, T. N. Blanton, R. H. Young, W. Brennessel, *J. Chem. Crystallogr.*, 2010, **40**, 195.
20 M. Rajeswaran, T. N. Blanton, C. W. Tang, W. C. Lenhart, S. C. Switalski, D. J. Giesen, B. J. Antalek, T. D. Pawlik, D. Y. Kondakov, N. Zumbulyadis, R. H. Young, *Polyhedron*, 2009, **28**, 835.
21 M. Colle, J. Gmeiner, W. Milius, H. Hillebrecht, W. Brutting, *Adv. Funct. Mater.*, 2003, **13**, 108.
22 H. Bi, H. Y. Zhang, Y. Zhang, H. Z. Gao, Z. M. Su, Y. Wang, *Adv. Mater.*, 2010, **22**, 1631.
23 P. Dera, C. T. Prewitt, S. Japel, D. L. Bish, C. T. Johnston, *Am. Mineral.*, 2003, **88**, 1428.
24 P. Destruel, P. Jolinat, R. Clergereaux, J. Farenc, *J. Appl. Phys*., 1999, **85**, 397.
25 I. Hernandez, W. P. Gillin, *J. Phys. Chem. B*, 2009, **113**, 14079.
26 I. Hernandez, W. P. Gillin M. Somerton, *J. Lumin.*, 2009, **129**, 1835.
27 Q. L. Wang, Y. H. Han, C. L. Liu, Y. Z. Ma, W. B. Ren, C. X. Gao, *Appl. Phys. Lett.*, 2012, **100**, 172905.
28 Y. Wang, Y. H. Han, C. X. Gao, Y. Z. Ma, C. L. Liu, G. Peng, B. J. Wu, B. Liu, T. J. Hu, X. Y. Cui, W. B. Ren, Y. Li, N. N. Su, H. W. Liu, G. T. Zou, *Rev. Sci. Instrum.*, 2010, **81**, 013904.
29 Mao, H. K.; Bell, P. M.; Shaner, J. W.; Steinberg, D. J. *J. Appl. Phys.* 1978, *49*, 3276-3283.
30 C. Y. He, C. X. Gao, Y. Z. Ma, M. Li, A. M. Hao, X. W. Huang, B. G. Liu, D. M. Zhang, C. L. Yu, G. T. Zou, Y. C. Li, H. Li, X. D. Li, J. Liu, *Appl. Phys. Lett.*, 2007, **91**, 092124.
31 R. Schmidt, J. Wu, C. Leighton, I. Terry, *Phys. Rev. B*, 2009, **79**, 125105.
32 J. C. C. Abrantes, J. A. Labrincha, J. R. Frade, *Mater. Res. Bull.*, 2000, **35**, 727.
33 I. Denk, J. Claus, J. Maier, *J. Electrochem. Soc*, 1997, **144**, 3526.
34 H. L. Tuller, *Solid State Ionic*s, 2000, **131**, 143.
35 A. P. Nayak, S. Bhattacharyya, J. Zhu, J. Liu, X. Wu, T. Pandey, C. Q. Jin, A. K. Singh, D. Akinwande, J.-F. Lin, *Nat. Commun.*, 2014, **5**, 3731.
36 T. Matsuoka, K. Shimizu, *Nature* 2009, **458**, 186.
37 Y. H. Hu, L. Zhang, *Phys. Rev. B* 2010, **81**, 174103.
38 I. Peral, J. Iniguez, *Phys. Rev. Lett.* 2006, **97**, 225502.
39 M. D. Halls, R. *Can.* Aroca, *J. Chem.*, 1998, **76**, 1730.
40 M. Braun, J. Gmeiner, M. Tzolov, M. Coelle, F. D. Meyer, W. Milius, H. Hillebrecht, O. Wendland, J. U. Von Schutz, W. Brutting, *J. Chem. Phys.*, 2001, **114**, 9625.
41 M. Zhou, K. Wang, Z. W. Men, C. L. Sun, Z. L. Li, B. B. Liu, G. T. Zou, B. Zou, *Cryt. Eng. Comm.*, 2014, **16**, 4084.
42 M. Zhou, M. J. Sun, Z. W. Men, Z. L. Li, T. C. Liu, Y. Z. Chen, S. N. Sun, C. L. Sun, S. Q. Gao, Z. W. Li, *J. Phys. Chem. B*, 2013, **117**, 8911.